Research Article Vol. 26, No. 14 | 9 Jul 2018 | OPTICS EXPRESS 18597

Optics EXPRESS

Illumination uniformity improvement in digital micromirror device based scanning photolithography system

ZHENG XIONG,[1,2,3] HUA LIU,[1,3,*] RONGHUAN CHEN,[1] JIA XU,[3] QIANKUN LI,[1] JINHUAN LI,[1] AND WENJUAN ZHANG[1]

[1]*Center for Advanced Optoelectronic Functional Materials Research, and Key Laboratory for UV-Emitting Materials and Technology of Ministry of Education, National Demonstration Center for Experimental Physics Education, Northeast Normal University, 5268 Renmin Street, Changchun 130024, China*

[2]*Department of Biomedical Engineering and Chemical Engineering, Syracuse University, Syracuse, NY 13244, USA*

[3]*State Key Laboratory of Applied Optics, Changchun Institute of Optics, Fine Mechanics and Physics, Chinese Academy of Sciences, Changchun 130033, China*

[*]*liuhua_rain@aliyun.com*

Abstract: Illumination uniformity in photolithography systems determines the dimensional difference across the entire lithographic substrate. However, traditional lithography system relies on expensive and complex illumination system for achieving uniform illumination. In this paper, we propose a simple and cost-effective method based on the modulation of digital micromirror device to improve illumination uniformity. The modulation according to a digital mask achieved via an iteration program improves the uniformity to be above 95%. We demonstrate the effectiveness of the method by experimentally fabricating a linear grating. By implementing this method, the maximum dimensional difference is decreased from 3.3μm to 0.3μm. Further simulations indicate that higher uniformity is achievable once the field of view on the DMD is divided into smaller subregions.

OCIS codes: (220.3740) Lithography; (220.4000) Microstructure fabrication; (150.2950) Illumination.

References and links

1. Z. Xiong, H. Liu, X. Q. Tan, Z. W. Lu, C. X. Li, L. W. Song, and Z. Wang, "Diffraction analysis of digital micromirror device in maskless photolithography system", J. Micro-Nanolitho., MEM **13**(4), 353–365 (2014).
2. W. Mei, "Point Array maskless lithography", US, 6473237B2 (2002).
3. K. Wu, T. Rindzevicius, M. S. Schmidt, K. B. Mogensen, S. Xiao, and A. Boisen, "Plasmon resonances of Ag capped Si nanopillars fabricated using mask-less lithography," Opt. Express **23**(10), 12965–12978 (2015).
4. J. B. Kim and K. H. Jeong, "Batch fabrication of functional optical elements on a fiber facet using DMD based maskless lithography," Opt. Express **25**(14), 16854–16859 (2017).
5. X.W. Guo, and Q.M. Dong, "Rapid fabrication of micro optical elements using DMD-based maskless lithography technique," Adv. Mater. Res., **146**, 143–146 (2011).
6. H. Wu, W. Hu, H. C. Hu, X. W. Lin, G. Zhu, J. W. Choi, V. Chigrinov, and Y. Q. Lu, "Arbitrary photo-patterning in liquid crystal alignments using DMD based lithography system," Opt. Express **20**(15), 16684–16689 (2012).
7. K. F. Chan, Z. Q. Feng, R. Yang, A. Ishikawa, and W. H. Mei, "High-resolution maskless lithography", J. Micro-Nanolitho., MEM **2**(4), 331–339 (2003).
8. M. P. Lee, G. J. T. Cooper, T. Hinkley, G. M. Gibson, M. J. Padgett, and L. Cronin, "Development of a 3D printer using scanning projection stereolithography," Sci. Rep. **5**(1), 9875 (2015).
9. W. H. Arnold, "Towards 3 nm overlay and critical dimension uniformity: an integrated error budget for double patterning lithography," SPIE **6924**, 692404 (2008).
10. A. Waldbaur, B. Waterkotte, K. Schmitz, and B. E. Rapp, "Maskless projection lithography for the fast and flexible generation of grayscale protein patterns," Small **8**(10), 1570–1578 (2012).
11. J. Kim, S. Bae, H. Lee, and S. Jang, "Maskless lithographic apparatus and methods of compensation for rotational alignment error using the same", US, 20100060874 (2010).
12. R. Voelkel, U. Vogler, A. Bich, P. Pernet, K. J. Weible, M. Hornung, R. Zoberbier, E. Cullmann, L. Stuerzebecher, T. Harzendorf, and U. D. Zeitner, "Advanced mask aligner lithography: new illumination system," Opt. Express **18**(20), 20968–20978 (2010).

#328009 https://doi.org/10.1364/OE.26.018597
Journal © 2018 Received 27 Apr 2018; revised 17 Jun 2018; accepted 20 Jun 2018; published 5 Jul 2018

Optics EXPRESS

13. M. Christophersen and B. F. Philips, "Gray-tone lithography using an optical diffuser and a contact aligner," Appl. Phys. Lett. **92**(19), 194102 (2008).
14. R. Hu, X. Luo, H. Zheng, Z. Qin, Z. Gan, B. Wu, and S. Liu, "Design of a novel freeform lens for LED uniform illumination and conformal phosphor coating," Opt. Express **20**(13), 13727–13737 (2012).
15. K. Zhong, Y. Gao, F. Li, N. Luo, and W. Zhang, "Fabrication of continuous relief micro-optic elements using real-time maskless lithography technique based on DMD," Opt. Laser Technol. **56**, 367–371 (2014).
16. R. Chen, H. Liu, H. Zhang, W. Zhang, J. Xu, W. Xu, and J. Li, "Edge smoothness enhancement in DMD scanning lithography system based on a wobulation technique," Opt. Express **25**(18), 21958–21968 (2017).
17. J. Ma, X. Du, and Y. Liu, "Design of maskless lithography system based on DMD," Proc. SPIE **6836**, 683612 (2008).
18. M. A. Klosner, "Maskless lithography system and method with doubled throughput", US, 6238852 (2001).
19. L. J. Hornbeck, "Deformable mirror spatial light modulators," Proc. SPIE **1150**, 86–104 (1990).
20. J. M. Younse, "Mirrors on a chip," IEEE Spectr. **30**(11), 27–31 (1993).
21. B. Sampsell, "Digital micromirror device and its application to projection displays," J. Vac. Sci. Technol. B **12**(6), 3242–3246 (1994).

1. Introduction

The interest of using digital micromirror device (DMD) to realize digital photolithography has been widely discussed in recent years. Compared with traditional lithography such as direct laser writing or mask lithography, DMD based photolithography demonstrates great advantages reaching higher throughput, micron/submicron resolution and lower cost [1–6]. Therefore, step and scanning lithography technique, fulfilled by the digital dynamic character of the DMD, is widely investigated for their ability to satisfy large-scale manufacturing such as printed circuit board (PCB), biochips or large-scale grating. To be more specific, scanning photolithography has become the mainstream as it provides the feasibility to minimize the pattern stitching error and on the other hand, avoids the requirement of a high-precision system alignment. What is more, the improvement of the DMD kit with a level of kHz frame frequency has made DMD based scanning photolithography mode feasible [7,8]. Nevertheless, even though the high performance of the DMD enables high precision lithography, the uniform illumination in the lithography system is critical as it directly determines the pattern dimensional difference across the entire substrate especially for the manufacture of large-scale patterns [9–11]. Under this scenario, three main methods used for achieving uniform illumination are proposed: (1) Köhler illumination using microlens array and xenon lamp [12]; (2) LED light source assembled with freeform lens; (3) lasers with diffuser or microlens array [13]. Unfortunately, apart from the fact that the expensive optical components are indispensable among the three above-proposed illumination schemes, the precise optical design is also required to realize the uniform illumination [14,15]. For instance, the price of a microlens array is over $600 (i.e., #64-478, Edmund Optics Inc.) and the estimated cost for the design and optimization of the corresponding illumination system with high uniformity is over $1000. Moreover, the illumination uniformity is not only influenced by the illumination system itself, but also by other factors such as laser speckle, nonuniform response of the DMD, defects of optical components and the alignment of the system. Therefore, a simple and cost-effective method to improve the illumination uniformity in a DMD scanning lithography system is favored.

In this framework, an illumination uniformity improvement technique implemented in the DMD scanning photolithography system, demonstrated as combining the DMD modulation (controlling on/off states of the micromirrors) with scanning lithography mode, is proposed. Afterwards, a theoretical model customized to the scanning photolithography mode, aiming at investigating the illumination uniformity effects on the dimensional difference, is established. Following this, simulation of patterned lines is proposed and the simulated results indicate that a dimensional difference of 4.8 μm is introduced by the nonuniform illumination. Hence, a digital mask optimization via an iteration program is proposed to improve the uniformity. By the correction of digital mask, the uniformity is improved to be above 95%. The feasibility of the method is demonstrated by fabricating a linear grating with a period of 10.8 μm.

Exposure results show that the maximum dimensional difference across the entire substrate is decreased from 3.3 μm to 0.3 μm.

2. DMD based scanning photolithography

2.1 Photolithography system

We first demonstrate a DMD based scanning photolithography system in Fig. 1 [16–18] which contains the laser diode (i.e., $\lambda = 405$nm), the illumination system, the DMD, the reflector, the projection lens and the lithographic substrate located on a precise scanning stage. The laser beam emitted from the laser diode is collimated and homogenized by the illumination system including an engineered diffuser (ED1-C20, Thorlabs) and an optical lens system (Doublets Lens, Edmund Optics). The light emitted from the laser diode is collimated by the optical system and then reflected to the DMD (0.95 inch 1080p UV-DMD, 1920 × 1080 with micromirror size of 10.68μm × 10.68μm, Texas Instruments) by a reflecting mirror. Note that the exposure pattern is sequentially displayed on the DMD by flipping the digital micromirrors. In this case, the modulated digital pattern is projected by the projection lens (1:1 ratio), and exposed on lithographic substrate (1.4 inch round glass) spin coated with SU8 photoresist (thickness of 0.3 mm). The scanning stage holding the lithographic substrate is moved at the speed of 10 mm/s controlled by the customized code.

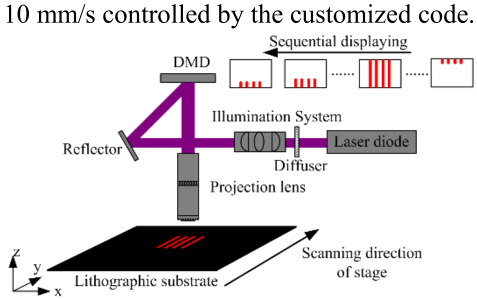

Fig. 1. Schematic of DMD based scanning photolithography system.

2.2 Mode of scanning photolithography

The key device in the above-mentioned system is the DMD consisting of a 2D micromirrors array [19–21]. The exposure pattern, which is a 2D pixilated figure, is displayed on the DMD through modulating the on/off states of the 2D micromirror arrays. The on/off states correspond to DMD's tilting angle + 12°/-12°. In this case, the micromirror with + 12° could pass through the projection lens and correspond to the exposed pixel on the lithographic substrate. The micromirror with −12° refers to the unexposed pixel. In the implementation of real scanning mode, the substrate is displaced by the scanning stage at a constant speed while the DMD is held static. The principle of the exposure mode is illustrated in Fig. 2. To help understand the mode, the DMD is simplified as a 5 × 5 array. In Figs. 2(1)-2(10), the modulated pattern is sequentially displayed on the DMD row by row to realize a scrolling display. The red squares and the white squares represent the micromirror of the DMD with + 12° and −12°, respectively. Accordingly, in Figs. 2(a)-2(j), the red squares and the black squares represent the exposed pixel and the unexposed pixel on the photoresist substrate, respectively. The digit in each square refers to times of exposure, which is equal to the number of micromirrors with the "on" state at the located position during the scanning process.

At this moment, we label the duration of any micromirror staying at one pixel as the exposure time and such exposure time is determined by the frame frequency of the DMD. To avoid the exposure mismatch between different pixels during the scanning process, the relationship between the scanning speed of stage and the DMD's frame frequency has to satisfy Eq. (1),

$$L = V \times f, \tag{1}$$

where L represents the size of the micromirror, V refers to the scanning speed of the stage and f is the frame frequency of the DMD.

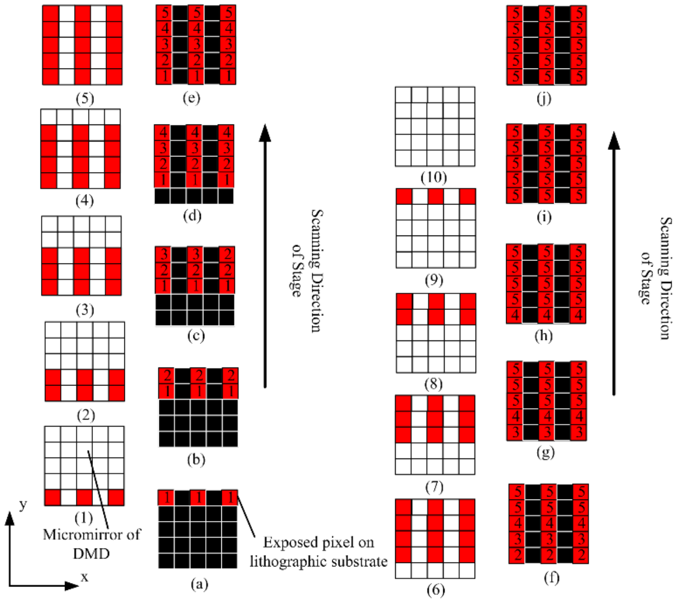

Fig. 2. Schematic of the mode of scanning photolithography.

Concerning the scheme shown in Fig. 2, the total exposure dose H_n at one exposed pixel on the substrate after the complete scanning process is correlated with the summation of $h_{m,n}$, which is the single exposure dose on this corresponding pixel within one scanning step. The summation is explained in Fig. 3. Note that the energy for single exposure dose is the reflected energy from light source by a single micromirror with the "on" state. Matrix A represents the distribution of the illumination, and matrix B corresponds to the distribution of the total exposure dose after the summation.

$$A = \begin{bmatrix} h_{1,1} & h_{1,2} \cdots\cdots & h_{1,n} \\ h_{2,1} & \ddots & \vdots \\ \vdots & & \\ h_{m,1} & \cdots\cdots & h_{m,n} \end{bmatrix} \downarrow \text{Summation}$$

$$\text{Eq. (2)} \downarrow$$

$$B = \begin{bmatrix} H_1 & H_2 & \cdots\cdots & H_n \end{bmatrix}$$

Fig. 3. Exposure dose of every pixel.

Therefore, H_n can be presented as:

$$H_n = \sum_{m=j}^{k} h_{m,n}, \tag{2}$$

where (m,n) represents the location of the micromirror with respect to the whole micromirror distribution, and the range (j,k) reveals the number of the micromirrors with the "on" states during the scanning exposure. For instance, the DMD in Fig. 2 is presented by a 5 × 5 array, therefore the total exposure dose H_1 received by the top left corner pixel in Fig. 2(j) is the summation of $h_{1,1}$, $h_{2,1}$, $h_{3,1}$, $h_{4,1}$ *and* $h_{5,1}$, here, j is 1 and k is 5.

Optics EXPRESS

In fact, the energy reflected by any "on" state micromirror to the substrate follows certain distribution of $I_{m,n}(x,y)$ which is considered as a 2D Gaussian shown as Eq. (3):

$$I_{m,n}(x,y) = P_{m,n} e^{-\left[\left(\frac{x}{a}\right)^2 + \left(\frac{y}{b}\right)^2\right]}, \tag{3}$$

where $P_{m,n}$ is the peak power of the Gaussian function, and the parameters a, b are the Gaussian radius which is considered equal to the size of a micromirror L.

Once the photolithography system is working under the linear scanning mode, the function of any single exposure dose $h_{m,n}(x,y)$ is an integration of $I_{m,n}(x,y)$:

$$h_{m,n}(x,y) = \int_0^L I_{m,n}(x, y+t)dt, \tag{4}$$

where t is the variable in the integration. We want to emphasize that the integral interval in Eq. (4) is L (i.e., size of micromirror) because this is the displacement distance of the stage along the scanning direction within one scanning step, For a better visualization of the integrating $h_{m,n}(x,y)$, we show the cross-section $h_{m,n}(0,y)$ of $h_{m,n}(x,y)$ along y axis (i.e., scanning direction) in Fig. 4.

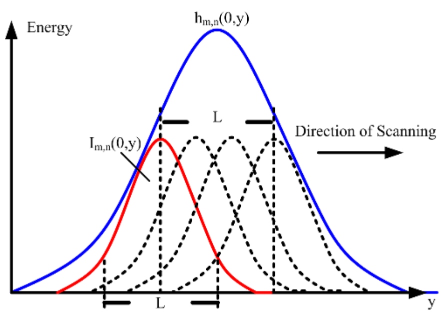

Fig. 4. Cross-section of $h_{m,n}(x,y)$ along y axis.

Finally, by substituting Eqs. (3) and (4) into Eq. (2), the total exposure dose H_n can be defined as:

$$H_n(x,y) = \sum_{m=j}^{k} P_{m,n} \int_0^L e^{-\left[\left(\frac{x}{a}\right)^2 + \left(\frac{y+t}{b}\right)^2\right]} dt. \tag{5}$$

3. Digital mask for illumination uniformity improvement

3.1 Effects of non-uniform illumination on dimensional difference

Note that H_n demonstrated in Eq. (5) directly determines the widths of the patterned line by assuming that the threshold of the photoresist is a constant. To be more specific, the two variables in Eq. (5), $P_{m,n}$ and the range *(j,k)* determine the total exposure dose H_n. Here, the range *(j,k)* reveals the number of the micromirrors with the "on" state at one column, which will be discussed later in section 3.2. Under this scenario, if *(j,k)* is considered as *(1,1080)* which means that all the micromirrors are at the "on" state, the only parameter deciding the total exposure dose (i.e., H_n) is $P_{m,n}$ which corresponds to the peak power of the Gaussian distribution. In the real implementation, $P_{m,n}$ is directly related to the illumination. Therefore, in Fig. 3, the distributuon of H_n (i.e., matrix B) decided by the distribution of $h_{m,n}$ (i.e., matrix A) could be considered being determined by the illumination distribution since a, b and L are constants, and then the illumination distribution decides the dimensional difference of patterned lines across the entire substrate.

Optics EXPRESS

For instance, we provide in Fig. 5(a) a non-uniform illumination captured by a grayscale camera at the imaging plane by implementing the DMD with all pixels adjusted to the "on" state. The corresponding distribution of total exposure dose realized by considering Eq. (5) is provided in Fig. 5(b). For characterizing the distribution of H_n, we define the uniformity as Eq. (6). The uniformity revealed by Fig. 5(b) is calculated as 78.62%.

$$Uniformity = \frac{Minimum}{Maximum}\%, \tag{6}$$

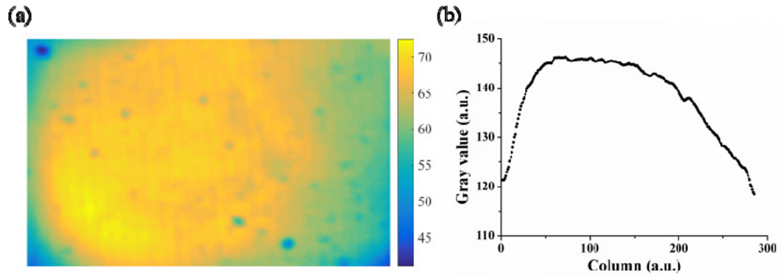

Fig. 5. (a) Grayscale image of non-uniform illumination, (b) Distribution of H_n.

To investigate the nonuniform illumination effect on dimensional difference, we implemented the numerical simulation of the patterned lines generated by the scanning exposure using Matlab by setting *a, b* (i.e., the Gaussian radius) and *L* (i.e., micromirror pixel size) all as 10.68 μm. We also define the scanning length of the exposure patterned lines as 10 pixels (~100 μm). The simulations are performed with the uniformities of 100% and 78.62% as shown in Figs. 6 and 7, respectively. We want to note that the widths of the patterned lines are decided by the uniformity and later are calculated at full width at half maximum (FWHM) along the *x* direction (perpendicular to the scanning direction). The simulated results of the patterned lines using the uniformities as 100% and 78.62% are as well demonstrated in Figs. 6 and 7, respectively. In Fig. 6, the simulated result shows that the line width difference can be totally eliminated if the uniformity of 100% is introduced. On the other hand, Fig. 7 reveals a simulated difference of line width as 4.8 μm, compared to the actual experimental exposure results demonstrate as 3.3 μm shown in Fig. 8. Both the simulated results and the experimental results obtained by the nonuniform illumination cannot meet the required precision in microfabrication.

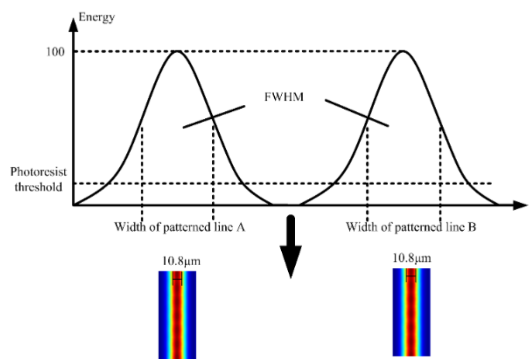

Fig. 6. Simulation under the uniformity with 100%.

Optics EXPRESS

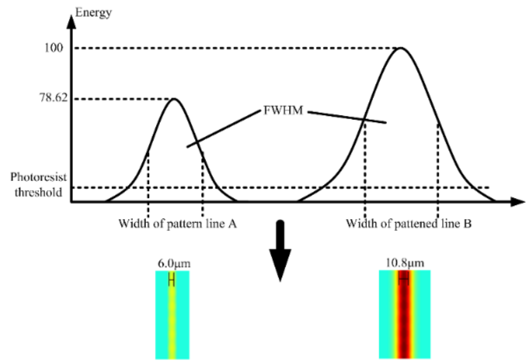

Fig. 7. Simulation under the uniformity with 78.62%.

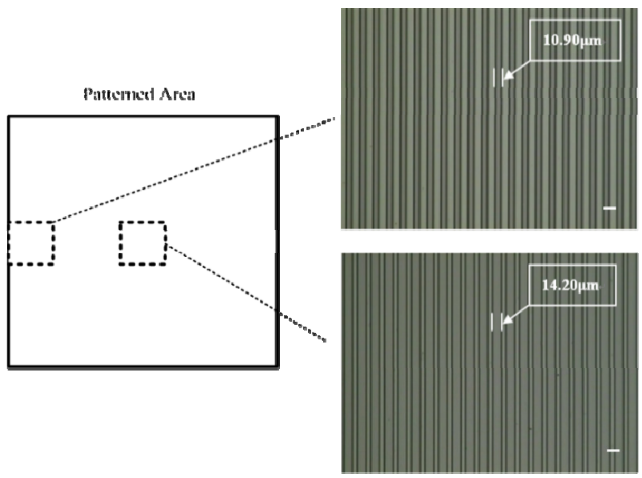

Fig. 8. Patterned lines in actual exposure experiments. Scale bar, 20µm.

3.2 Digital mask for improvement of nonuniform illumination

In order to achieve uniform patterned lines across the whole substrate, a correction method is mandatory to improve the non-uniform illumination. As it is demonstrated in Section 3.1, two variables $P_{m,n}$ and *(j,k)* influence the total exposure dose (i.e., H_n) and therefore introduce the dimensional difference of the pattern width. We want to note that one variable $P_{m,n}$ is determined by the illumination characteristic. Therefore, the other variable *(j,k)* is the key factor to improve the illumination uniformity. In fact, *(j,k)* is directly determined by the displayed pattern modulated by the DMD. Under this scenario, we propose a DMD based digital mask which only controls the range *(j,k)* (selectively set some pixels as the "off" state) to improve the nonuniform illumination.

We want to highlight that the energy distribution demonstrated in Fig. 5 in fact is not feasible to be used to optimize the digital mask directly. This is because the energy distribution captured by the camera without a precise calibration (i.e., eliminating the noise effects arise from the camera and the environment) is not adequately accurate to be applied in the further correction. What is more, it is also not efficient to collect the energy from each micromirror on the DMD. Therefore, we assume that the energy in a small area (less than 5 mm^2) is uniform, we then simplify the whole field of view on the DMD by divided it into a 10 × 10 distributed subregions. Note that the location of each subregion is represented by (*p,q*) with respect to the whole subregion distribution. Afterwards, the energy at each subregion is measured for 10 times using a powermeter calibrated by the integrating sphere, and the final energy of each subregion is calculated by averaging these 10 energy measurements. Here the

Optics EXPRESS

exposure energy of any subregion is defined as $e_{p,q}$. The 10 × 10 distributed matrix A^* with different $e_{p,q}$ values represents the simplified illumination distribution. Not that the matrix is to be used in the following process in Fig. 10 to obtain digital mask. By using the Eq. (5), the corresponding simplified distribution of total exposure dose H^*_n is calculated and shown in Fig. 9. It is obviously demonstrated that the energy in the central part is higher than the side parts, which matches the corresponding patterned lines results illustrated in Fig. 8. The uniformity of H^*_n is 71.52%.

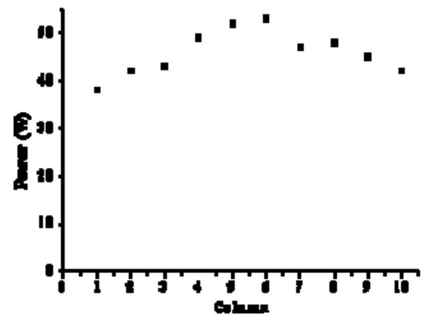

Fig. 9. Distribution of H^*_n before correction.

According to the analysis above, by DMD based digital mask to control the range of *(j,k)* (selectively closing some pixels), the uniformity of the distribution H_n can be improved. Therefore, we use this same principle to improve the uniformity of the simplified distribution of H^*_n. Here, the maximum range of *(j,k)* is *(1,10)* (i.e., the range of subregions). Controlling *(j,k)* means selectively closing one certain subregion at each column of matrix A^*. The DMD based digital mask provides this optimal selection which could improve the uniformity of H^*_n. The flow chart in Fig. 10 presents the process for generating the DMD based digital mask. In step *(1,1)*, the subregions except for those in column 1 and the subregion *(1,1)* are closed (marked as black in Fig. 10) and thus the range *(j,k)* revealing the remaining subregions with the "on" state is left as *(2,10)*. Then the total exposure energy of the rest 9 subregions is $E_{1,1}$. In step *(p,q)*, the subregion *(p,q)* is closed and the total exposure energy of the rest 9 subregions is $E_{p,q}$. Note that the term $E_{p,q}$ introduced here demonstrates the total exposure energy of any step. $E_{p,q}$ is finally illustrated by Eq. (7):

$$\text{Step}(p,q):\text{except for} e_{p,q}, \tag{7}$$

The exposure energy calculated at whole steps (i.e., from step *(1,1)* to step *(10,10)*) are obtained and presented in a 10 × 10 matrix M shown in Fig. 10. Note that the 10 values in every column of matrix M (i.e., matrix of $E_{p,q}$) are obtained by sequential closing one subregion in the corresponding column of matrix A^*. For instance, in first column of matrix M, the values from $E_{1,1}$ to $E_{10,1}$ are obtained by sequential closing a subregion from *(1,1)* to *(10,1)* respectively in the column 1 of matrix A^*. But we can only close one subregion at each column as mentioned above. Therefore these 10 values in each column of matrix M provide 10 alternative choices. Every value corresponds to a potential choice for H^{**}_n. We need to find one certain value from each column and then form an optimal combination which has the highest uniformity. The locations *(p,q)* of these chosen values provide the digital mask modulated by DMD. Here, an iterative algorithm for searching the optimal combination is applied into the matrix M, and this algorithm is described below. First, we select the maximum element in the whole matrix M, which is located in a certain column, and then we select other nine values with the minimum difference value compared to this maximum in each of the rest nine columns. Afterwards, the uniformity of the ten values is calculated using Eq. (6) and is compared with our expected uniformity indicator (i.e., 95%). If it is greater than

95%, then the iteration is terminated and the locations in matrix M of the ten values are recorded for constructing the digital mask, otherwise the iteration is to be continuously executed to the second loop. We then select the secondary maximum and continue to compare it with the rest nine values in the nine remaining columns, which is the same as it in the first loop. The uniformity obtained from this second loop is also introduced to be compared with the indicator 95%. This iteration continues until the uniformity greater than 95% is found. However, another situation is to be encountered by assuming that there is no result being found with the uniformity above 95%. In this case, we choose the one with the highest uniformity. Eventually, as it is mentioned above, the final combination is the distribution of optimized exposure energy H^{**}_n and its locations *(p,q)* reveals the digital mask. The uniformity is improved from 71.52% to 95.17%, and the distribution of H^{**}_n is shown in Fig. 11.

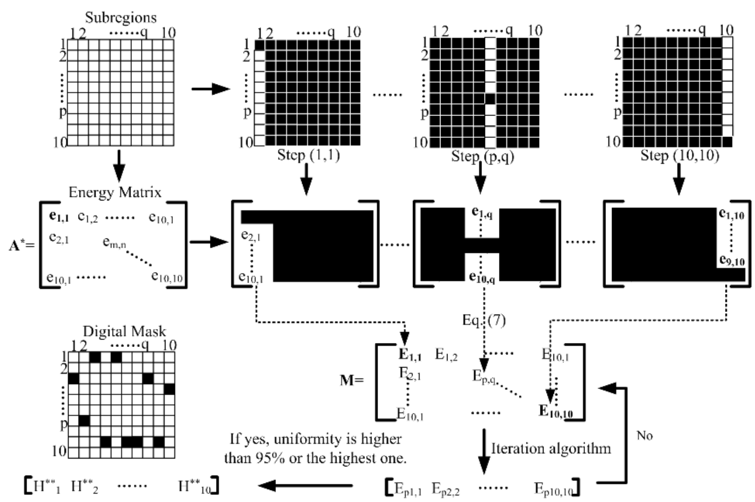

Fig. 10. Flow chart for obtaining digital mask.

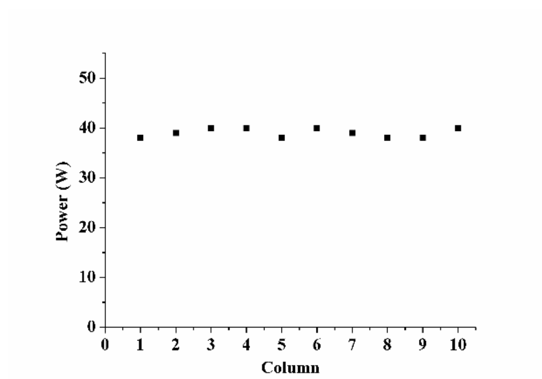

Fig. 11. Distribution of H^{**}_n after correction by digital mask.

4. Experimental results

Exposure experiments are performed to verify the effectiveness of the proposed digital mask by implementing the flow chart from step *(1,1)* to step *(10,10)* presented in Fig. 10. During each step, we close the micromirrors at the black subregions and implement the exposure for 10 times under the scanning mode. The patterned line width is measured and recorded by an optical microscope. The line width of each step by averaging 10 width measurements is recorded in the matrix shown in Table 1. Then the 10 values with minimum dimensional

Optics EXPRESS

difference are chosen from each column in Table 1 and highlighted. We want to note that the distribution of the chosen values in the matrix of Table 1 shares the same pattern as the digital mask being shown in Fig. 10. Moreover, we also extract the figures of the patterned line generated after being optimized by the digital mask at the same position as it in Fig. 8 and present them in Fig. 12. The maximum line width difference is dramatically improved from 3.3 μm to 0.3 μm, which verifies the feasibility of the proposed method.

Table 1. Patterned line width (μm)

	Column									
Row	1	2	3	4	5	6	7	8	9	10
1	9.80	9.86	**10.90**	11.02	**11.15**	11.84	12.10	10.50	10.56	10.24
2	10.48	10.54	10.16	10.96	11.32	12.06	11.80	10.52	10.94	10.82
3	**10.85**	10.12	10.00	10.44	11.26	12.00	11.82	**10.80**	10.50	11.04
4	10.27	10.22	9.90	10.85	11.20	11.82	11.18	11.44	10.32	**10.75**
5	10.12	9.92	10.14	10.50	11.17	11.80	11.96	11.74	11.08	10.32
6	10.24	10.42	10.10	10.78	11.18	12.08	12.08	10.68	10.50	10.22
7	9.98	**10.75**	10.06	10.62	11.26	11.72	11.46	11.42	11.24	10.28
8	10.05	10.12	9.92	10.44	11.20	11.10	12.20	10.42	11.02	10.18
9	9.56	10.28	9.94	**10.80**	11.20	**11.05**	**11.05**	11.44	**10.82**	10.18
10	10.43	10.42	10.00	10.60	11.16	11.90	12.10	10.76	10.84	10.20

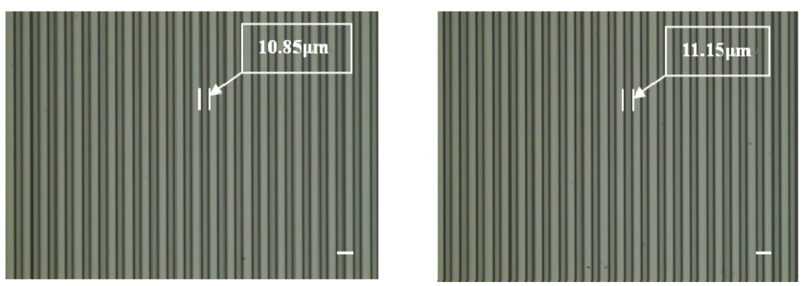

Fig. 12. Patterned lines after improvement by 10 × 10 digital mask. Scale bar, 20 μm.

At last, note that the field of view on the DMD is divided by 10 × 10 subregions and the dimensional difference of the patterned lines is decreased from 3.3 μm to 0.3 μm. To further investigate the proposed uniformity correction technique, we also calculate the uniformity improvement with different models of subregion distribution including the 5 × 5, the 6 × 6, the 8 × 8 and the 20 × 20 models and their corresponding uniformity are shown in Fig. 13. It is obvious that the uniformity is improved by increasing the number of the subregions. However, the 5 × 5 case presents a uniformity reduction as the energy of each subregion could not be considered as uniform since the area (~10.3 mm^2) of the subregion is too large. Another unexpected uniformity reduction illustrated by the 20 × 20 subregions distribution is caused by the fact that this digital mask has not been optimized based on the previous mask (10 × 10 subregions based mask). Once this 20 × 20 subregions distribution is optimized by using the optimized energy matrix from the 10 × 10 subregions case, the uniformity is improved to 95.92% (red dot in Fig. 13). Even though the uniformity increment is not obvious by comparing the 10 × 10 case with the 20 × 20 case, it is expectable that we could achieve a higher uniformity if the energy matrix is subdivided into smaller subregions such as 50 × 50 or 100 × 100. Since our exposure results based on 10 × 10 sub regions has achieved 0.3 μm dimensional difference, it has satisfied the requirement of our system. Considering the efficiency of energy measurements for the models of 50 × 50 and 100 × 100, we chose the case of 10 × 10 subregions as relatively optimal choice.

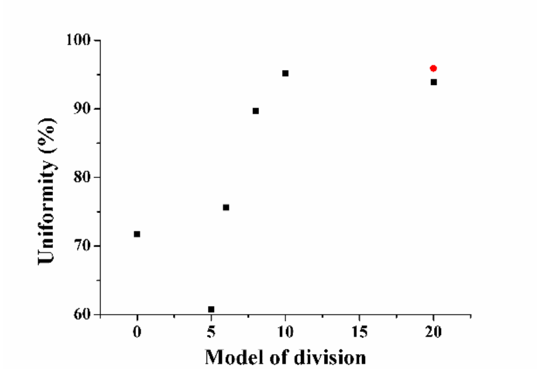

Fig. 13. Relationship between uniformity and model of division.

5. Conclusion

In this paper, a simple and cost-effective illumination uniformity improving technique implemented in a DMD based scanning photolithography system is proposed. Instead of using expensive optical components and complicate optical system, we improve the illumination uniformity by taking the benefit of combining the DMD modulation technique with an iteration algorithm for the digital mask optimization. The practicality of this technique is verified by implementing the actual exposure experiments. The experimental results show that the maximum dimensional difference is dramatically reduced from 3.3 μm to 0.3 μm. Therefore, such proposed illumination uniformity correction method could be used to improve the illumination non-uniformity effects on dimensional difference in DMD based scanning photolithography systems. Moreover, this technique provides the feasibility to enhance the uniformity, from which a higher uniformity is expedient, if the energy matrix could be subdivided into smaller subregions.

Funding

Jilin Province Youth Leading Talent and Team Project (20160519021JH).

Acknowledgments

This work is supported by the Innovation of Science and Technology in Jilin Province Youth Leading Talent and Team Project (20160519021JH) and the State Key Laboratory of Applied Optics. We thank Haolin Zhang from Universitat Autonoma de Barcelona for his useful comments on manuscript preparation.